AD-A153 850 A STUDY OF AERODYNAMIC CONTROL IN STALLED FLIGHT LONG LAMINAR SEPARATION. (U) ANALYTICAL METHODS INC REDMOND WA F A DVORAK ET AL. FEB 85 AFWAL-TR-84-3091 1/1

UNCLASSIFIED F33615-81-C-3626 F/G 20/4 NL

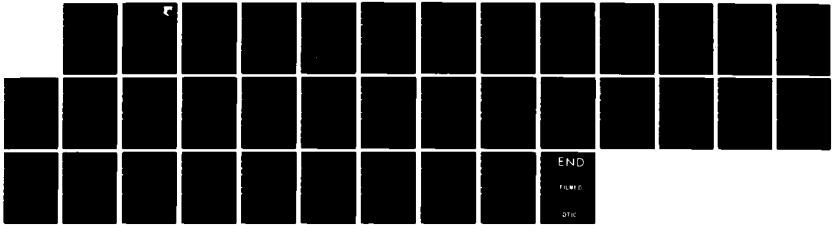

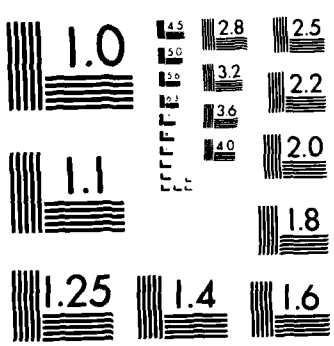

AFWAL-TR-84-3091

A STUDY OF AERODYNAMIC CONTROL IN STALLED FLIGHT
LONG LAMINAR SEPARATION BUBBLE ANALYSIS

F.A. Dvorak and D.H. Choi
ANALYTICAL METHODS, INC.
2047 - 152nd Avenue N.E.
Redmond, Washington 98052

February 1985

Final Report for Period December 1981 - August 1984

FLIGHT DYNAMICS LABORATORY
AIR FORCE WRIGHT AERONAUTICAL LABORATORIES
AIR FORCE SYSTEMS COMMAND
WRIGHT-PATTERSON AIR FORCE BASE, OHIO 45433

NOTICE

When Government drawings, specifications, or other data are used for any purpose other than in connection with a definitely related Government procurement operation, the United States Government thereby incurs no responsibility nor any obligation whatsoever; and the fact that the government may have formulated, furnished, or in any way supplied the said drawings, specifications, or other data, is not to be regarded by implication or otherwise as in any manner licensing the holder or any other person or corporation, or conveying any rights or permission to manufacture use, or sell any patented invention that may in any way be related thereto.

This report has been reviewed by the Office of Public Affairs (ASD/PA) and is releasable to the National Technical Information Service (NTIS). At NTIS, it will be available to the general public, including foreign nations.

This technical report has been reviewed and is approved for publication.

WILLIAM B. BLAKE
Project Engineer

VERNON O. HOENHE
Chief, Control Dynamics Branch
Flight Control Division

FOR THE COMMANDER

FRANK A. SCARDINO
Chief, Flight Control Division

"If your address has changed, if you wish to be removed from our mailing list, or if the addressee is no longer employed by your organization please notify AFWAL/FIGC, W-PAFB, OH 45433 to help us maintain a current mailing list".

Copies of this report should not be returned unless return is required by security considerations, contractual obligations, or notice on a specific document.

Unclassified

SECURITY CLASSIFICATION OF THIS PAGE

AD-A153850

REPORT DOCUMENTATION PAGE

1a. REPORT SECURITY CLASSIFICATION: Unclassified	1b. RESTRICTIVE MARKINGS: None
2a. SECURITY CLASSIFICATION AUTHORITY	3. DISTRIBUTION/AVAILABILITY OF REPORT: Approved for public release; distribution unlimited.
2b. DECLASSIFICATION/DOWNGRADING SCHEDULE	
4. PERFORMING ORGANIZATION REPORT NUMBER(S)	5. MONITORING ORGANIZATION REPORT NUMBER(S): AFWAL-TR-84-3091
6a. NAME OF PERFORMING ORGANIZATION: Analytical Methods, Inc. / 6b. OFFICE SYMBOL (If applicable)	7a. NAME OF MONITORING ORGANIZATION: AF Flight Dynamics Laboratory AFWAL (AFSC)
6c. ADDRESS (City, State and ZIP Code): 2047 152nd Ave N.E. Redmond WA 98052	7b. ADDRESS (City, State and ZIP Code): Wright-Patterson AFB OH 45433
8a. NAME OF FUNDING/SPONSORING ORGANIZATION: AFOSR / 8b. OFFICE SYMBOL (If applicable): NA	9. PROCUREMENT INSTRUMENT IDENTIFICATION NUMBER: F33615-81-C-3626
8c. ADDRESS (City, State and ZIP Code): Bolling AFB DC 20332	10. SOURCE OF FUNDING NOS.

PROGRAM ELEMENT NO.	PROJECT NO.	TASK NO.	WORK UNIT NO.
61102F	2307	N3	25

11. TITLE (Include Security Classification): A Study of Aerodynamic Control in Stalled Flight Long Laminar Separation Bubble Analysis

12. PERSONAL AUTHOR(S): Dvorak, Frank A. and Choi, D.H.

13a. TYPE OF REPORT	13b. TIME COVERED	14. DATE OF REPORT (Yr., Mo., Day)	15. PAGE COUNT
Final	FROM Dec 81 TO Aug 84	1985 February	28

16. SUPPLEMENTARY NOTATION

17. COSATI CODES			18. SUBJECT TERMS (Continue on reverse if necessary and identify by block number)
FIELD	GROUP	SUB. GR.	Panel Methods, Boundary Layer, Laminar Separation Bubble
01	01		
01	02		

19. ABSTRACT (Continue on reverse if necessary and identify by block number)

This report describes an analysis method for laminar separation bubbles (long or short) on two-dimensional air foil sections at incidence. A viscous/potential flow iterative procedure was chosen due to its simple and efficient nature. The boundary layer procedure is a finite-difference method, sometimes referred to as the "Box Scheme", and uses the Cebeci-Smith two-layer, eddy-viscosity model for turbulence closure. The potential flow is calculated by a low order panel method, where each panel is represented by a constant potential surface. The laminar separation bubble is modelled in the potential flow calculation in such a way that it gives constant pressure along the surface inside the bubble. The coupled calculation procedure has been applied to the NACA 64A006 airfoil and satisfactory results have been obtained.

20. DISTRIBUTION/AVAILABILITY OF ABSTRACT	21. ABSTRACT SECURITY CLASSIFICATION
UNCLASSIFIED/UNLIMITED ☒ SAME AS RPT. ☐ DTIC USERS ☐	Unclassified

22a. NAME OF RESPONSIBLE INDIVIDUAL	22b. TELEPHONE NUMBER (Include Area Code)	22c. OFFICE SYMBOL
William B. Blake	513-255-8484	AFWAL/FIGC

DD FORM 1473, 83 APR EDITION OF 1 JAN 73 IS OBSOLETE.

Unclassified

SECURITY CLASSIFICATION OF THIS PAGE

TABLE OF CONTENTS

SECTION		PAGE NO.
1.0	INTRODUCTION	1
2.0	POTENTIAL FLOW CALCULATION METHOD	2
	2.1 Modelling of the Separation Bubble	5
3.0	BOUNDARY LAYER CALCULATION PROCEDURE	
	3.1 Basic Equations	6
	3.2 Closure Model for Turbulent Flow	7
	3.3 Transition from Laminar to Turbulent Boundary Layer . .	8
	3.3.1 Granville's Transition Cirterion	8
	3.3.2 Crimi/Reeves' Criterion	10
	3.4 Finite-Difference Scheme	11
	3.5 Solution Procedure	
	3.5.1 Standard Boundary Layer Calculation	12
	3.5.2 Inverse Boundary Layer Calculation	13
	3.5.3 Initial Velocity Profile	14
	3.5.4 Grid Distribution across the Boundary Layer . .	14
4.0	VISCOUS/POTENTIAL FLOW ITERATION	15
5.0	RESULTS AND DISCUSSION	17
6.0	RECOMMENDATIONS FOR FUTURE WORK	26
7.0	REFERENCES	27

LIST OF FIGURES

FIG. NO.	TITLE	PAGE NO.
1	Integration Domain	2
2	Flow in the Vicinity of Separation Bubble	10
3	Finite-Difference Grid for the Box Scheme	11
4	Schematic of Calculation Procedure	16
5	Pressure Distribution after Two Full Viscous/Potential Iterations; NACA 64A006, $\alpha = 5^0$, Re = 5.8 x 10^6 (Fixed Transition)	18
6	Pressure Distribution after Two Full Viscous/Potential Iterations; NACA 64A006, $\alpha = 6^0$, Re = 5.8 x 10^6 (Fixed Transition)	19
7	Effect of Separation Model in the Potential Flow Calculation	20
8	Overall Pressure Distribution on NACA 64A006; $\alpha = 5^0$, Re = 5.8 x 10^6	21
9	Overall Pressure Distrubution on NACA 64A006; $\alpha = 6^0$, Re = 5.8 x 10^6	22
10	Overall Pressure Distribution on NACA 64A006; $\alpha = 7^0$ . .	23
11	C_ℓ - α Curve for an Airfoil Section NACA 64A006; Re = 5.8 x 10^6	24

LIST OF SYMBOLS

A	Eddy viscosity constant of Eq. (21a)
a_{ij}	Aerodynamic influence matrix
b	$1 + \varepsilon^{+}$
b_i	Right-hand side of discretized integral equation
C	Surface boundary of potential flow
C_p	Pressure coefficient
F	Stream function (Eq. (18))
h_j	Grid spacing normal to surface
k	Eddy viscosity constant of Eq. (21a)
k_i	Grid spacing tangent to surface
n	Normal to surface
P	Pressure
R	Reynolds number based on the length given as a subscript
r_{st}	Distance between surface points, s and t
s	Point on flow boundary
t	Point on flow boundary
U_e	Velocity external to boundary layer
u	x-component of velocity
v	Transpiration velocity or y-component of velocity
x_{tr}	x of boundary layer transition

LIST OF SYMBOLS (CONCLUDED)

γ_{tr} Intermittency factor

δ Boundary layer thickness

δ^* Displacement thickness

ε^+ Eddy viscosity

θ Momentum thickness

λ Non-dimensional pressure gradient

ν Kinematic viscosity

ρ Density

τ_w Surface shear stress

ϕ Total potential of flow

ϕ Disturbance potential of flow

Subscripts

sep Separation

TEL Trailing edge, lower

TEU Trailing edge, upper

tr Transition

∞ Conditions at infinity

1.0 INTRODUCTION

A detailed knowledge of the flow around an airfoil leading edge is critical to the understanding of the stall phenomena. In an early study by McCullough and Gault (1), various types of stall were discussed and extensive data were presented for several NACA airfoil sections. More recently, Roberts (2) described the phenomenon and proposed a semiempirical theory for the separation bubble. Some investigators have tried to calculate the separated region directly by using inverse boundary layer technique. These attempts have been quite successful in obtaining correlation with experiment (see Refs. 3 and 4). However, these methods are valid only for small bubbles (less than 2% chord) and the application to larger bubbles has not been particularly successful.

The current study was undertaken to develop an analysis method for laminar separation bubbles (long or short) on two-dimensional airfoil sections at incidence. A viscous/potential flow iterative procedure was chosen due to its simple and efficient nature. This view has recently been confirmed by Johnson et al. (5); i.e., that a good inverse boundary layer calculation method is as accurate as the more time-consuming Navier-Stokes methods in predicting the separated flow.

In the present work, Cebeci's boundary layer calculation method (6), which is capable of predicting separated flow by an inverse boundary layer calculation procedure, is coupled with the potential flow calculation method developed earlier, VS2D (7). The boundary layer procedure is a finite-difference method, sometimes referred to as the "Box Scheme", and uses the Cebeci-Smith two-layer, eddy-viscosity model for turbulence closure. The potential flow is calculated by a low-order panel method where each panel is represented by a constant potential surface. The laminar separation bubble is modelled in the potential flow calculation in such a way that it gives constant pressure along the surface inside the bubble.

The coupled calculation procedure has been applied to the NACA 64A006 airfoil and satisfactory results have been obtained. The details of the solution procedure and comparisons with experiment are fully described in this report.

2.0 POTENTIAL FLOW CALCULATION METHOD

The velocity potential of a two-dimensional body in a uniform flow (unit velocity in x-direction) in the rectangular Cartesian coordinate system is given by:

$$\Phi(x,y) = x + \phi(x,y) \tag{1}$$

where ϕ is the disturbance velocity potential. The solid surface boundary condition gives $\partial\phi/\partial n = 0$; i.e.,

$$\frac{\partial \phi}{\partial n} = - \frac{\partial x}{\partial n} \tag{2}$$

From Green's identity, the disturbance velocity potential on the boundary can be expressed as

$$\phi_s = \frac{1}{\pi} \int_C \left[\phi_t \frac{\partial}{\partial n_t} \left(\ell n \frac{1}{r_{st}} \right) - \left(\ell n \frac{1}{r_{st}} \right) \frac{\partial \phi}{\partial n_t} \right] dt \tag{3}$$

where s and t denote points on the boundary and r_{st} represents the distance between the two points as shown in Figure 1.

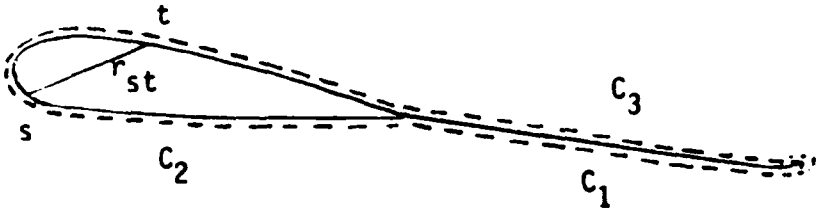

Figure 1. Integration Domain.

The integration domain of Eqn. (3) includes the thin sheet which extends from the trailing edge to infinity in order to account for the discontinuity in potential at the trailing edge.

Substitute Eqn. (2) into (3) to obtain

$$\phi_s = \frac{1}{\pi} \int_C \phi_t \frac{\partial}{\partial n_t}(\ell n \frac{1}{r_{st}})dt + \frac{1}{\pi} \int_C \frac{\partial x}{\partial n_t} \ell n(\frac{1}{r_{st}})dt \tag{4}$$

or

$$\phi_s = \frac{1}{\pi} \int_{C_1+C_2+C_3} \phi_t \frac{\partial}{\partial n_t}(\ell n \frac{1}{r_{st}})dt + \frac{1}{\pi} \int_{C_1+C_2+C_3} \frac{\partial x}{\partial n_t} \ell n(\frac{1}{r_{st}})dt \tag{4a}$$

Since the Kutta condition requires upper and lower surface velocities to be equal at the trailing edge, the velocity potential, ϕ, along the paths, C_1 and C_3, may be written as

$$\begin{aligned} \phi_U &= \phi_{T.E.U} + \left.\frac{\partial \phi}{\partial t}\right|_{T.E.} \cdot (t - t_{T.E.}) \\ \phi_L &= \phi_{T.E.L} + \left.\frac{\partial \phi}{\partial t}\right|_{T.E.} \cdot (t - t_{T.E.}) \end{aligned} \tag{5}$$

Thus, the contributions from the second term, $\left.\frac{\partial \phi}{\partial t}\right|_{T.E.} \cdot (t - t_{T.E.})$, and from the second integral along the paths C_1 and C_3 are cancelled out. This leaves us with

$$\begin{aligned} \phi_s = \frac{1}{\pi} \int \left[\phi_t \frac{\partial}{\partial n_t}(\ell n \frac{1}{r_{st}}) + \frac{\partial x}{\partial n_t} \ell n(\frac{1}{r_{st}}) \right] dt \\ + \frac{1}{\pi} \phi_{T.E.L} \int \frac{\partial}{\partial n_t}(\ell n \frac{1}{r_{st}})dt + \frac{1}{\pi} \phi_{T.E.U} \int \frac{\partial}{\partial n_t}(\ell n \frac{1}{r_{st}})dt \end{aligned} \tag{6}$$

This is an integral equation of the second kind and the solution can be found easily using a simple integration technique.

In the present method, the contour is approximated by a number of linear surface panels and ϕ assumes a constant value on each element. With this approximation, the contribution from each surface element can be calculated analytically and, hence, converts the integral equation, Eqn. (6), into a system of linear equations.

$$a_{ij}\,\phi_j = b_i \tag{7}$$

Having obtained ϕ, the velocity on the surface can be readily obtained by a simple differentiation.

$$u(t) = \frac{\partial \Phi}{\partial t} = \frac{\partial x}{\partial t} + \frac{\partial \phi}{\partial t} \tag{8}$$

It is useful to note that the boundary layer displacement effect, which may be expressed as the velocity component normal to the surface, can be easily incorporated in the calculation by modifying the boundary condition, Eqn. (2).

$$\frac{\partial \Phi}{\partial n} = v$$

or

$$\frac{\partial \phi}{\partial n} = v - \frac{\partial x}{\partial n} \tag{9}$$

where v is the transpiration velocity.

2.1 Modelling of the Separation Bubble

The separation bubble is represented by a constant pressure region in the potential flow calculation; i.e.,

$$C_p = C_p\Big|_{sep} \tag{10}$$

or

$$\left(\frac{\partial \Phi}{\partial s}\right)^2 + v^2 = \left[\left(\frac{\partial \Phi}{\partial s}\right)^2 + v^2\right]_{sep} \tag{11}$$

where Φ is the total potential and v is the transpiration velocity. However, if this condition is imposed in addition to Eq. (7), a proper ϕ distribution may not exist for a given distribution of v, which satisfies both Eq. (7) and (11) simultaneously. In other words, the system is overdetermined. The correct ϕ which satisfies both equations can be obtained only if v is compatible with ϕ. In the present work, this is achieved in the following manner.

Consider Eq. (3).

$$\phi_s = \frac{1}{\pi} \int_C \left[\phi_t \frac{\partial}{\partial n_t} \left(\ell n \frac{1}{r_{st}}\right) - \left(\ell n \frac{1}{r_{st}}\right) \frac{\partial \phi}{\partial n_t}\right] dt \tag{3}$$

where

$$\frac{\partial \phi}{\partial n_t} = v - \frac{\partial \phi_\infty}{\partial n_t}$$

First, solve for ϕ for a given distribution of v. Here, Eq. (3) or (7) and (11) are used for the attached flow region and the bubble region, respectively. Once ϕ is calculated, the new v distribution can be obtained from Eq. (3). Note that Eq. (3) is an integral equation of the first kind for v. If this v is the same as that of the previous iteration, then ϕ and v are considered to be compatible. By repeating this procedure, the ϕ and corresponding v distributions can be obtained.

3.0 BOUNDARY LAYER CALCULATION PROCEDURE

3.1 Basic Equations

The coordinate system employed in the boundary layer analysis is a body-fitted surface coordinate system (x,y), i.e., one coordinate, x, is parallel to the surface and the other, y, is normal to the surface. This is a natural choice for the solution of boundary layer equations on a two-dimensional airfoil as it doesn't exhibit any singular behavior around the leading edge. In such a coordinate system, the first-order boundary layer equations are:

$$\text{Continuity:} \quad \frac{\partial u}{\partial x} + \frac{\partial v}{\partial y} = 0 \tag{12}$$

$$\text{Momentum:} \quad u \frac{\partial u}{\partial x} + v \frac{\partial u}{\partial y} = - \frac{1}{\rho} \frac{dp}{dx} + \nu \frac{\partial}{\partial y} \left[(1 + \varepsilon^+) \frac{\partial u}{\partial y} \right] \tag{13}$$

where ε^+ is dimensionless eddy viscosity, ε/ν.

Equations (12) and (13) are subject to the usual boundary conditions, namely,

$$\left.\begin{aligned} u &= v = 0 \quad \text{at} \quad y = 0 \\ u &= U_e \\ v &= 0 \end{aligned}\right\} \quad \text{at} \quad y = \delta \tag{14}$$

Now dimensionless variables are introduced:

$$\bar{u} = u/U_\infty, \qquad \bar{v} = v/U_\infty \cdot \sqrt{R_L}, \qquad \bar{p} = p/\rho U_\infty^2$$

$$\bar{x} = x/L, \qquad \bar{y} = y/L \cdot \sqrt{R_L}, \qquad R_L = U_\infty L/\nu \tag{15}$$

where L and U_∞ are reference length and velocity, respectively.

Substituting these new variables in Eqs. (12) and (13) yields

$$\frac{\partial \bar{u}}{\partial x} + \frac{\partial \bar{v}}{\partial y} = 0 \tag{16}$$

$$\bar{u} \frac{\partial \bar{u}}{\partial x} + \bar{v} \frac{\partial \bar{u}}{\partial y} = - \frac{d\bar{p}}{dx} + \frac{\partial}{\partial y} \left[b \frac{\partial \bar{u}}{\partial y} \right] \tag{17}$$

where $b = 1 + \epsilon^+$.

Introducing a stream function, defined as

$$\bar{u} = \frac{\partial F}{\partial y}, \qquad \bar{v} = - \frac{\partial F}{\partial x} \tag{18}$$

Equations (16) and (17), after dropping the bars for convenience, may be written as

$$(b\, F'')' = \frac{dp}{dx} + F' \frac{\partial F'}{\partial x} - F'' \frac{\partial F}{\partial x} \tag{19}$$

Here primes denote differentiation with respect to y.

Equation (19) can then be converted to a system of first-order differential equations and can be solved by using a finite-difference scheme with appropriate boundary conditions and initial condition. The details of the solution procedure will be discussed in a later section. For laminar flow calculations, the term ϵ^+ in Eq. (13) has no meaning and is given a zero value.

3.2 Closure Model for Turbulent Flow

A simple eddy viscosity model, "zero-equation" model, is used as a closure relationship. In this model, Reynolds stress is given by

$$-\overline{u'v'} = \epsilon \frac{\partial u}{\partial y} \tag{20}$$

where ε is the eddy viscosity. Here the variation of ε across the boundary layer is prescribed in two parts as proposed by Cebeci and Smith (Ref. 9):

Inner Layer

$$\varepsilon_i = \left| \kappa y \left[1 - \exp(-y/A) \right] \right|^2 \left| \frac{\partial u}{\partial y} \right| \qquad \varepsilon_i \leq \varepsilon_o \tag{21a}$$

Outer Layer

$$\varepsilon_o = 0.0168 \left| \int_0^\infty (U_e - u)\, dy \right| \tag{21b}$$

where $\kappa = 0.4$, $A = 26\nu/u_\tau$, and $u_\tau = \sqrt{\tau_w/\rho}$.

The transition effects are taken into account by multiplying ε by the intermittency factor, γ_{tr}, based on Emmon's hypothesis that the transition phenomenon in a boundary layer is characterized by the intermittent appearance of turbulent spots which move downstream with the fluid:

$$\gamma_{tr} = 1 - \exp\left[-\frac{1}{1200} R_{x_{tr}}^{0.66} \left(\frac{x}{x_{tr}} - 1 \right)^2 \right] \tag{22}$$

3.3 Transition from Laminar to Turbulent Boundary Layer

Two transition criteria are employed in the boundary layer analysis. Granville's procedure (Ref. 10) is used for attached flow, and transition in the separated region is predicted by Crimi/Reeves' criterion (Ref. 11).

3.3.1 Granville's Transition Criterion

Granville (Ref. 10) has developed a procedure based on the relationship between the neutral stability point and the transition point. The neutral stability point is defined as a point downstream of which small disturbances are amplified within the boundary layer and ultimately lead to transition. Smith (Ref. 12) and others here proposed the correlation between the instability curve and the local pressure gradient, $\lambda = \theta^2/\nu \cdot dU/dx$, as follows:

$$\lambda = -0.4709 + 0.11066\ \ell n\ R_\theta - 0.0058591\ \ell n^2 R_\theta \qquad 0 < R_\theta \leq 650 \qquad (23)$$

$$\lambda = 0.69412 - 0.23992\ \ell n\ R_\theta + 0.0205\ \ell n^2 R_\theta \qquad 650 < R_\theta \leq 10{,}000 \qquad (24)$$

If for a given R_θ, λ as calculated by Eqns. (23) and (24) is greater than that determined by the boundary layer development, the flow has passed from a stable to an unstable region. Once the flow passes into the unstable region, the transition process begins, and Granville has been able to show that a correlation similar to the instability process can be used to determine the transition point.

Granville formed an average pressure gradient parameter, $\bar{\lambda}$, defined as

$$\bar{\lambda} = \frac{\int_{x_{ins}}^{x_{tr}} \lambda\ dx}{x_{tr} - x_{ins}} \qquad (25)$$

which correlated reasonably well with the momentum thickness Reynolds number at transition $R_{\theta_{trans}}$. This correlation is presented in analytical form as follows:

Transition Curves

$$\bar{\lambda} = -0.0925 + 7.0 \times 10^{-5}\ R_\theta \qquad (26)$$

for $0 < R_{\theta_{tr}} \leq 750$;

$$\bar{\lambda} = -0.12571 + 1.14286 \times 10^{-4}\ R_\theta \qquad (27)$$

for $750 < R_{\theta_{tr}} \leq 1100$;

and $$\bar{\lambda} = 1.59381 - 0.45543\ \ell n\ R_\theta + 0.032534\ \ell n^2\ R_\theta \qquad (28)$$

$$\text{for} \quad 1100 < R_{\theta_{tr}} \leq 3000.$$

When the $\bar{\lambda}$ calculated by one of the above expressions for a given R_θ is greater than the value determined from the boundary layer development, transition is predicted.

3.3.2 Crimi/Reeves' Criterion

If the laminar boundary layer separates prior to transition, then the following relationship is used to predict the onset of transition as proposed by Crimi and Reeves (Ref. 11),

$$\frac{y\big|_{u=0}}{\delta^*_{sep}} = \frac{10^6}{\left[R_{\delta^*}\right]^2_{sep}} \qquad (29)$$

where δ^* is the boundary layer displacement thickness and the subscript, "sep", denotes the quantity at the separation point (see Figure 2).

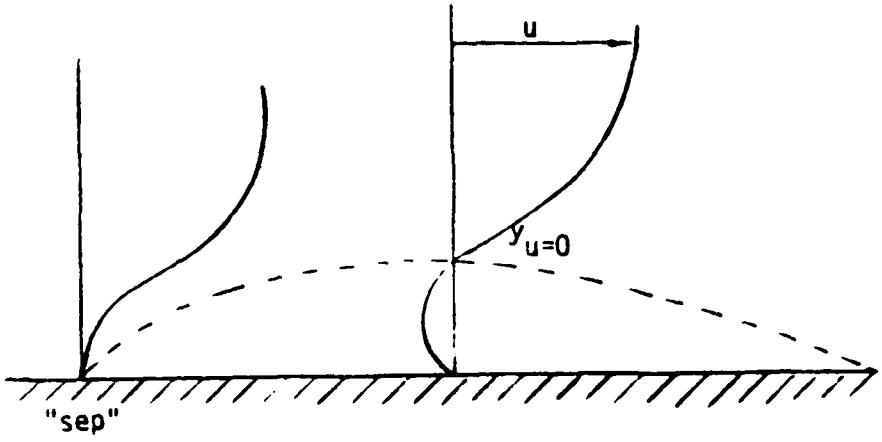

Figure 2. Flow in the Vicinity of Separation Bubble.

3.4 Finite-Difference Scheme

The finite-difference formulation used here is an implicit method originated by Keller (Ref. 8) and is referred to as the Keller Box method.

Consider a simple second-order parabolic equation,

$$\frac{\partial u}{\partial x} = \frac{\partial^2 u}{\partial y^2} = u'' \tag{30}$$

This equation can be reduced to a system of first-order equations by substituting $v = u'$; i.e.,

$$u' = v \tag{31}$$

$$v' = \frac{\partial u}{\partial x} \tag{32}$$

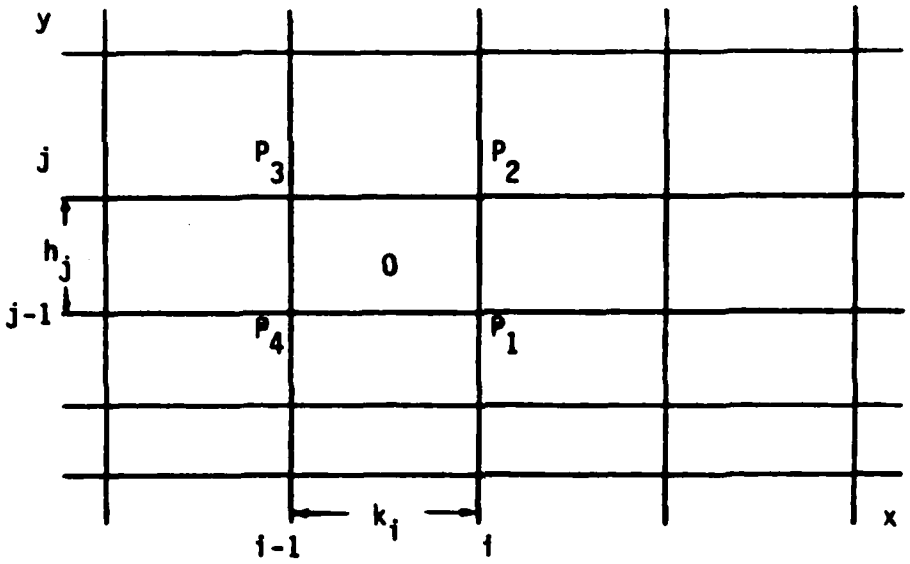

Figure 3. Finite-Difference Grid for the Box Scheme.

The difference equations used to approximate Eqns. (31) and (32) about the point, 0, the center of the rectangle, $P_1P_2P_3P_4$, in Figure 3, may be written as follows:

$$\frac{U_j^i - U_{j-1}^i}{h_j} = V_{j-\frac{1}{2}}^i \qquad (33)$$

$$\frac{(V')^i + (V')^{i-1}}{2} = \frac{U^i - U^{i-1}}{k_i} \qquad (34a)$$

Equation (34a) can be further discretized as

$$\frac{1}{2h_j}\left(V_j^i - V_{j-1}^i + V_j^{i-1} - V_{j-1}^{i-1}\right) = \frac{1}{2k_i}\left(U_j^i + U_{j-1}^i - U_j^{i-1} - U_{j-1}^{i-1}\right) \qquad (34b)$$

or

$$V_j^i - V_{j-1}^i - \frac{h_j}{k_i}\left(U_j^i + U_{j-1}^i\right) = -V_j^{i-1} + V_{j-1}^{i-1} - \frac{2h_j}{k_i} U_{j-\frac{1}{2}} \qquad (34c)$$

Equations (33) and (34c) together with boundary conditions form a block tri-diagonal matrix equation and can be readily solved for U and V by the block elimination method (Ref. 13).

The accuracy of this method is of second order and its implicit nature provides unconditional stability for any choice of x-step size.

3.5 Solution Procedure

3.5.1 Standard Boundary Layer Calculation

As shown earlier, the present "Box" scheme requires the differential equations to be of first order. By introducing new independent variables, $u(x,y)$ and $v(x,y)$, Eq. (19) can be transformed into a system of first-order equations as follows:

$$F' = u$$

$$u' = v$$

$$(b_1 v)' = \frac{dp}{dx} + u\,\frac{\partial u}{\partial x} - v\,\frac{\partial F}{\partial x} \qquad (35)$$

The usual boundary conditions, non-slip condition at the wall and free-stream condition at the outer edge of the boundary layer, are given by

$$F = 0,\ u = 0 \quad \text{at} \quad y = 0$$

$$u = U_e \quad \text{at} \quad y = \delta \qquad (36)$$

These represent basic equations for the standard boundary layer calculation procedure and can be readily solved by the method described earlier.

3.5.2 Inverse Boundary Layer Calculation

Equations (35) become singular at the separation point and, therefore, the above solution procedure fails as the flow approaches separation. This difficulty can be avoided if a different set of boundary calculations are specified; i.e.,

$$F = 0,\ u = 0 \quad \text{at} \quad y = 0$$

$$F = U_e(y - \delta^*) \quad \text{at} \quad y \to \infty \qquad (37)$$

In this inverse mode, U_e comes out as part of solutions and need not be specified. This is an iterative procedure that is repeated until the calculated δ^* matches the specified one.

For flows with negative wall shear, it is necessary to make approximations to the governing equations to continue the calculations past the separation point. The approximation used here neglects the $u(\partial u/\partial x)$ term in the region of negative u-velocity as originally suggested by Reyhner and Flügge-Lotz (Ref. 14).

3.5.3 Initial Velocity Profile

The calculation starts from the forward stagnation point with the Hiemenz-Howarth two-dimensional stagnation profile (Ref. 15) as an initial condition.

3.5.4 Grid Distribution across the Boundary Layer

The computation domain in the direction normal to the surface extends from the wall, where the no-slip condition applies, to some point beyond the edge of the boundary layer, where the velocity component, u, approaches its potential flow value, U_e. Typically, 51 to 61 grid points are distributed across this domain. Additional grid points are added as the boundary layer grows to ensure that the whole boundary layer lies within the integration domain. The node points are redistributed whenever the number of points reaches the prescribed maximum (61 in the present case).

The distribution of these grid points is nonuniform, with the spacing denser near the surface. The use of nonuniform grid spacing across the layer is essential for turbulent flow calculations. This can be achieved by using a grid which has the property that the ratio of lengths of any two adjacent intervals is a constant; i.e., $h_j = Ch_{j-1}$. The distance to the j^{th} line is given by the following formula:

$$y_j = h_1(C^j - 1)/(C - 1) \qquad C > 1 \tag{38}$$

The total number of points J can be calculated from the expression

$$J = \frac{\ell n[1 + (C - 1)\frac{y_J}{h_1}]}{\ell nC} \tag{39}$$

where y_J is the outer limit of the integration domain.

4.0 VISCOUS/POTENTIAL FLOW ITERATION

Initially, the potential flow solution is obtained with or without the separation bubble specified by the procedure described in an earlier section. This potential flow solution, mainly velocity distribution, is used in the calculation of the boundary layer development. The attached flow solution starts from the stagnation point and proceeds until it predicts the separation. If a turbulent separation is predicted, then the boundary layer calculation stops and the calculation returns to the potential flow routines. If the calculation predicts a laminar separation along the upper surface of the wing, the solution continues with the inverse boundary layer method. The boundary layer displacement thickness distribution which is required for the inverse calculation is prescribed initially--later this will be correlated with the normal velocity distribution in the potential flow calculation--so that the calculation can continue until the flow reattaches. Reattachment is possible because of transition to the turbulent flow inside the bubble. The section downstream of the reattachment point is calculated by a standard boundary layer method. This completes one full viscid/inviscid iteration cycle (see Figure 4).

The calculation returns to the beginning and repeats the procedure. Now the normal velocity due to the boundary layer displacement effect can be incorporated in the potential flow calculation. The whole procedure is considered to be converged when the external velocity along the bubble matches that of the potential flow and the reattachment point does not move from one iteration to another.

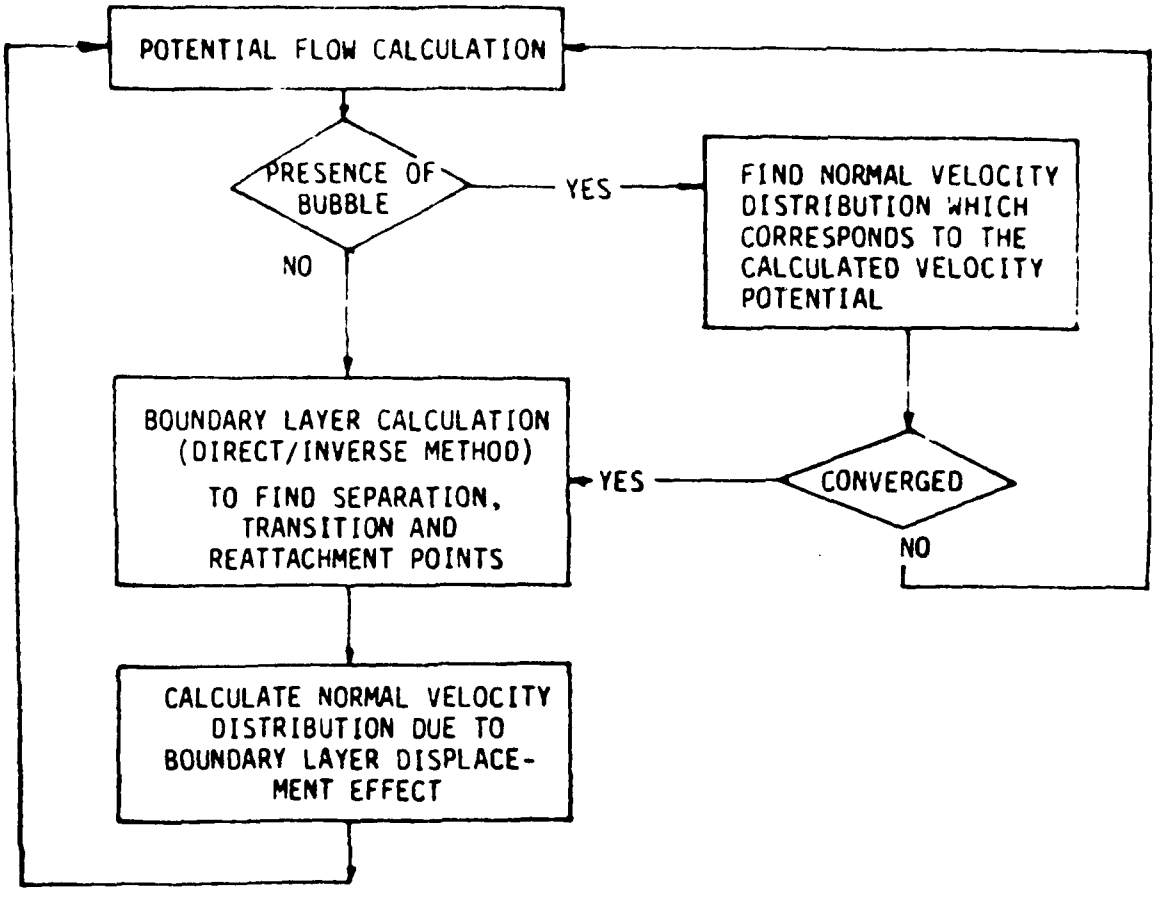

Figure 4. Schematic of Calculation Procedure.

5.0 RESULTS AND DISCUSSION

The experimental study of laminar separation bubbles on an airfoil section has been pursued by only a small number of investigators and, consequently, few adequate data sets for comparison are available in the literature.

Gaster (16) generated a separation bubble on a flat plate by artificially applying an adverse pressure gradient and was successful in measuring the characteristics of laminar separation bubbles; i.e., pressure, velocity profiles, etc. However, since one of the prime objectives of the present study is modeling of the separation bubble in the potential flow calculation, this case was not considered. The data by Gault (17) for various airfoil sections are limited to small bubbles and not suitable for the present work. In 1951, McCullough and Gault conducted an experimental study on the leading-edge bubble for various airfoil sections. Among the data obtained by McCullough/Gault, the data on the airfoil section NACA 64A006 were chosen for comparison because of the medium range bubble sizes (3 - 20%) which are of current interest.

Figures 5 and 6 are the results of two full viscous/potential flow iterations for $\alpha = 5°$ and $6°$, respectively. Figure 7 shows the pressure distribution for $\alpha = 7°$ just after the potential flow calculation with the separation model. All the solutions are started with the flow fully attached and the boundary layer analysis (both direct and inverse methods) determines the laminar separation, transition and reattachment points. In this separation bubble analysis, the location of transition is very important as the bubble model is applied from the separation point to the transition point. The transition procedure adopted here (Crimi/Reeves) tends to predict early transition. It is possible that the velocity profile on which the separation criterion is based may be in error or the procedure itself may not be adequate for long bubbles. This subject could not be examined thoroughly during the current phase of the work due to limited resources and deserves further study. In order to avoid any uncertainties in this repect, the onset of transition is fixed in the present calculations.

As shown in Figures 5 and 6 the boundary layer solution for the first iteration is not close to either the potential flow solution on the experimental data. However, with the aid of the separation model, these solutions quickly converge in the second iteration. Figure 7 shows a slight discrepancy in the transition/reattachment region between the potential flow solution and the data. This is due to the transition process which is not an abrupt process as modelled in the potential flow calculation. This view is confirmed by the fact that the boundary layer solutions are in better agreement with the experimenta data, as a result of the more gradual transition process, than is the potential flow calculation with its separation model.

As pointed out earlier, it is apparent from these results that the size of the bubble is of critical importance to the prediction of the correct pressure level along the surface of the separation bubble. It is also useful to note that the flow does not exhibit trailing-edge separation, and the pressure correlation for the rest of the airfoil is very good as shown in Figures 8 through 10. The C_ℓ - α curve comparison is plotted in Figure 11 and the correlation is very encouranging.

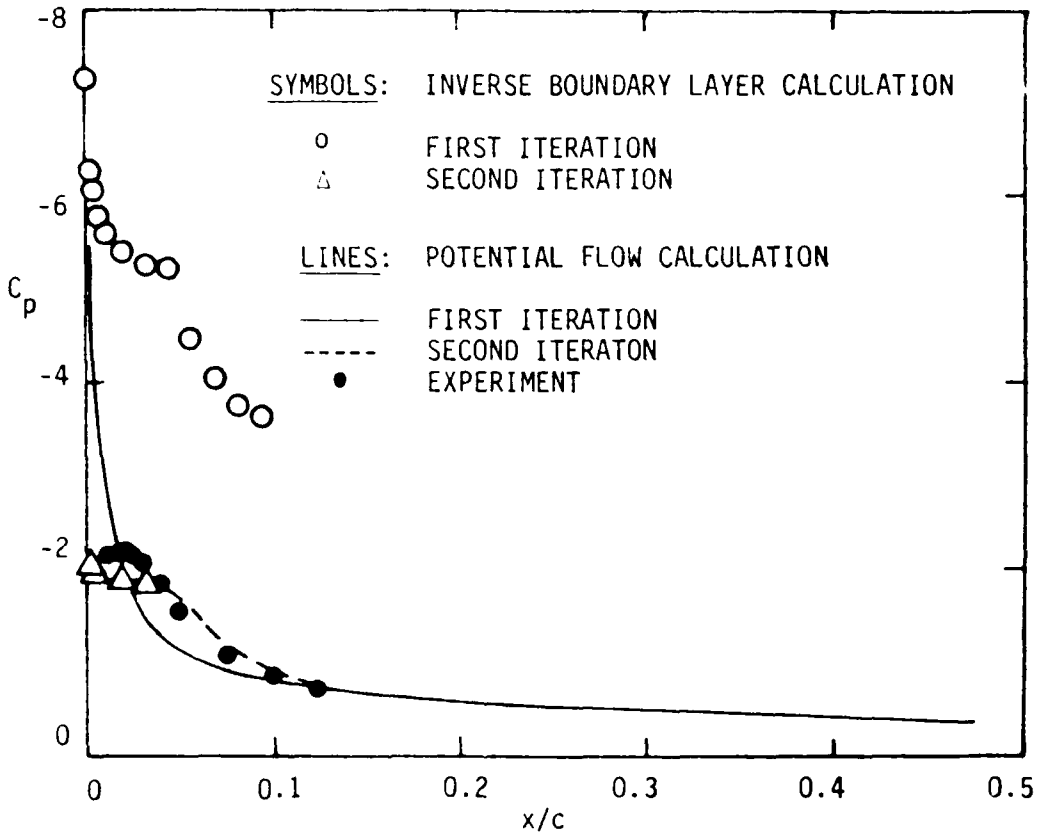

Figure 5. Pressure Distribution after Two Full Viscous/Potential Iterations; NACA 64A006, $\alpha = 5°$, Re = 5.8 x 10^6 (Fixed Transition).

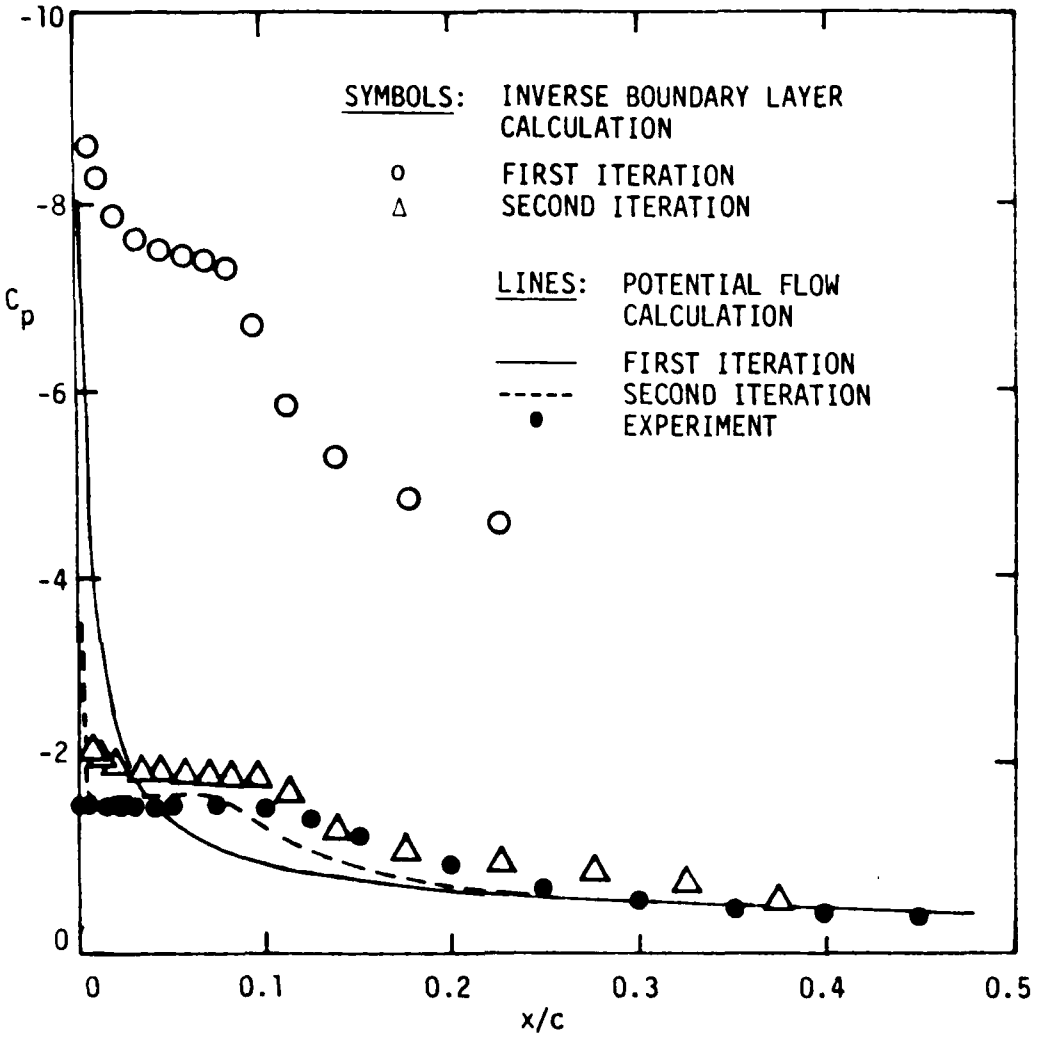

Figure 6. Pressure Distribution after Two Full Viscous/Potential Iterations; NACA 64A006, $\alpha = 6°$, Re = 5.8×10^6 (Fixed Transition).

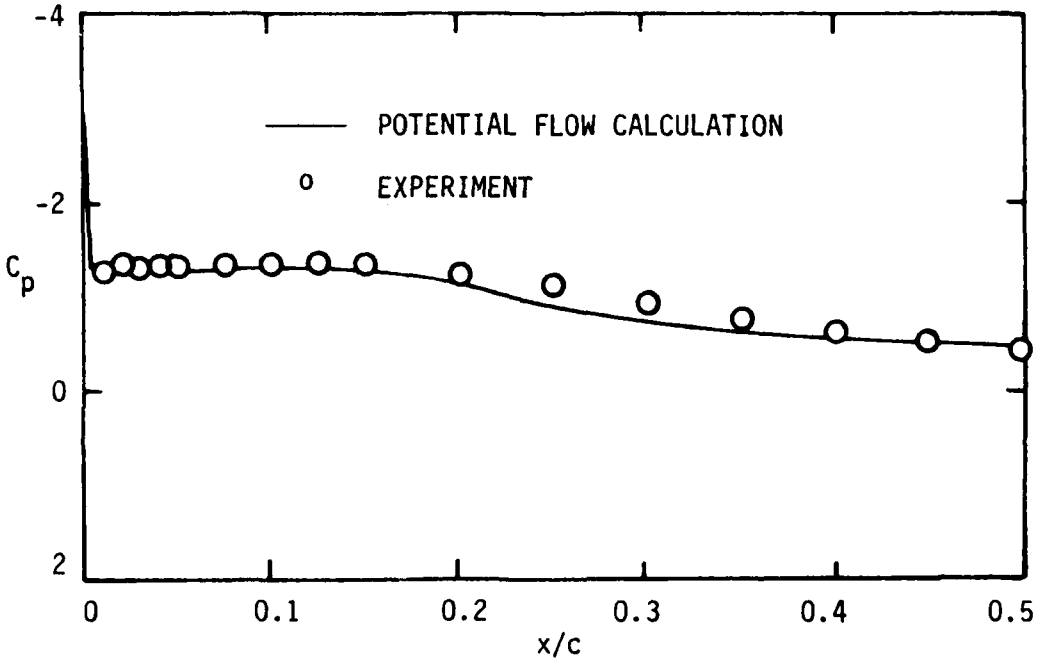

Figure 7. Effect of Separation Model in the Potential Flow Calculation.

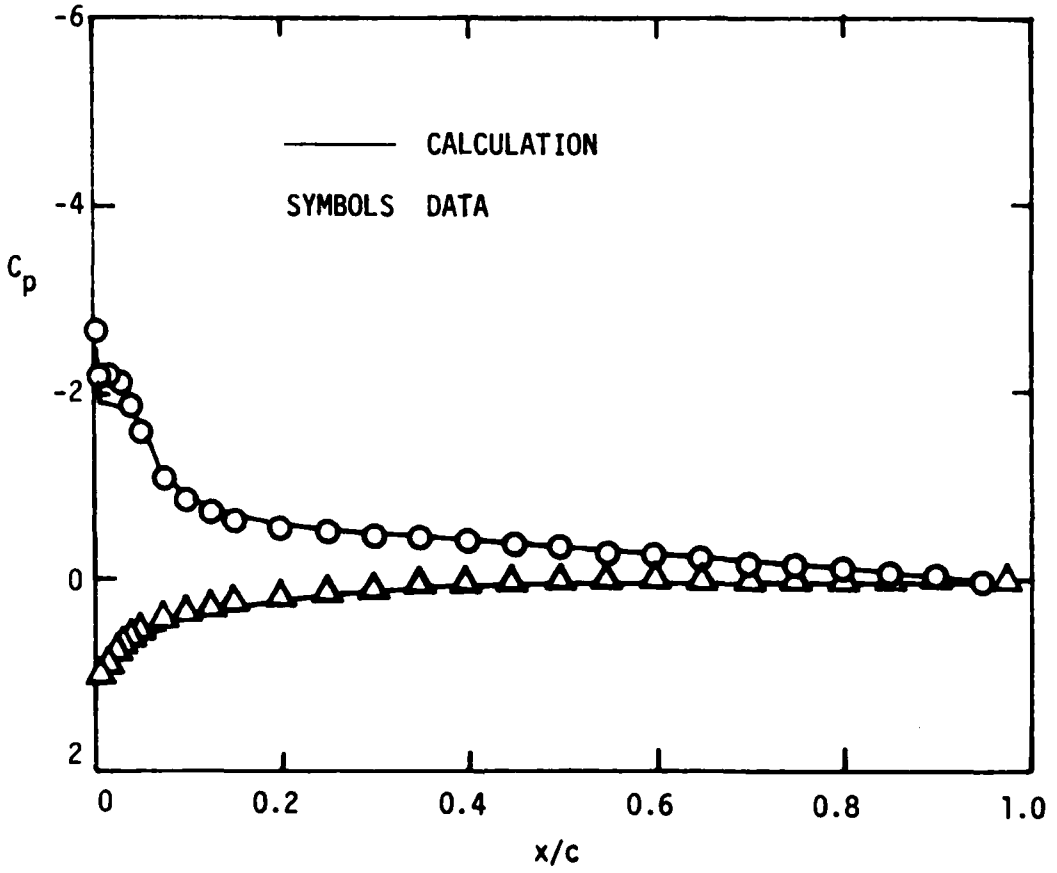

Figure 8. Overall Pressure Distribution on NACA 64A006; $\alpha = 5°$, $Re = 5.8 \times 10^6$.

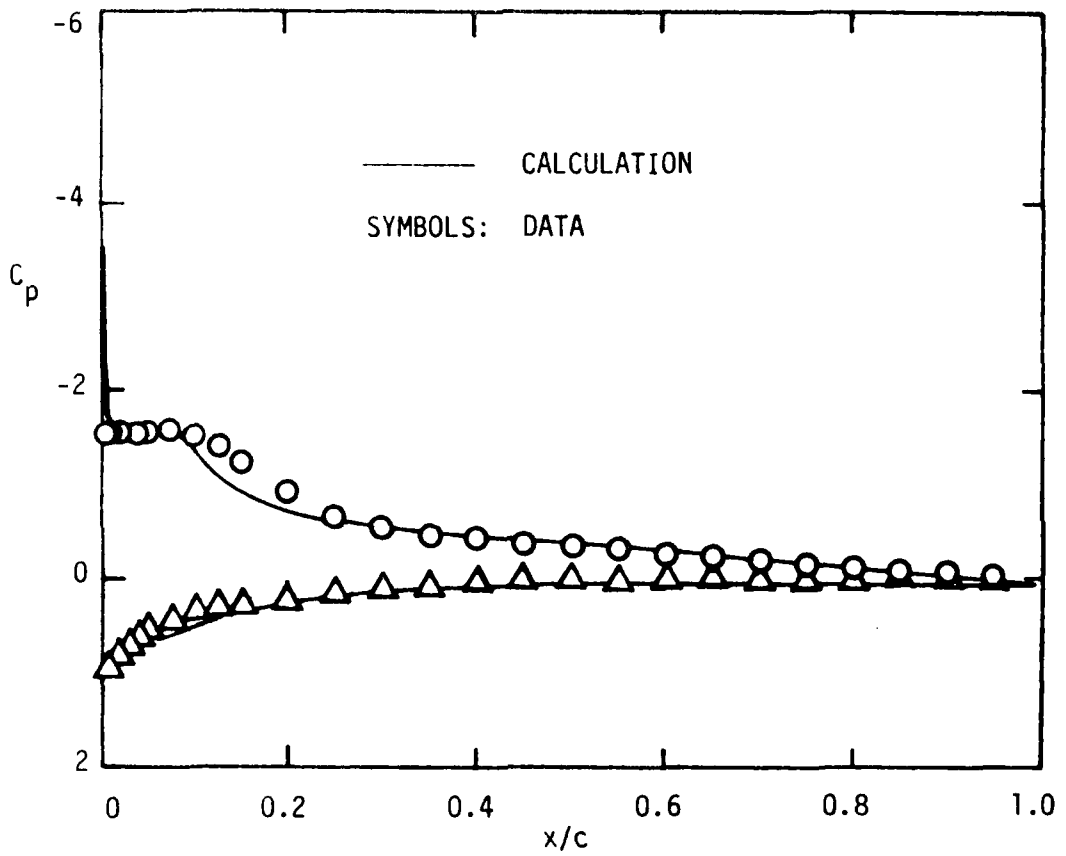

Figure 9. Overall Pressure Distribution on NACA 64A006; $\alpha = 6°$, Re = 5.8 x 10^6.

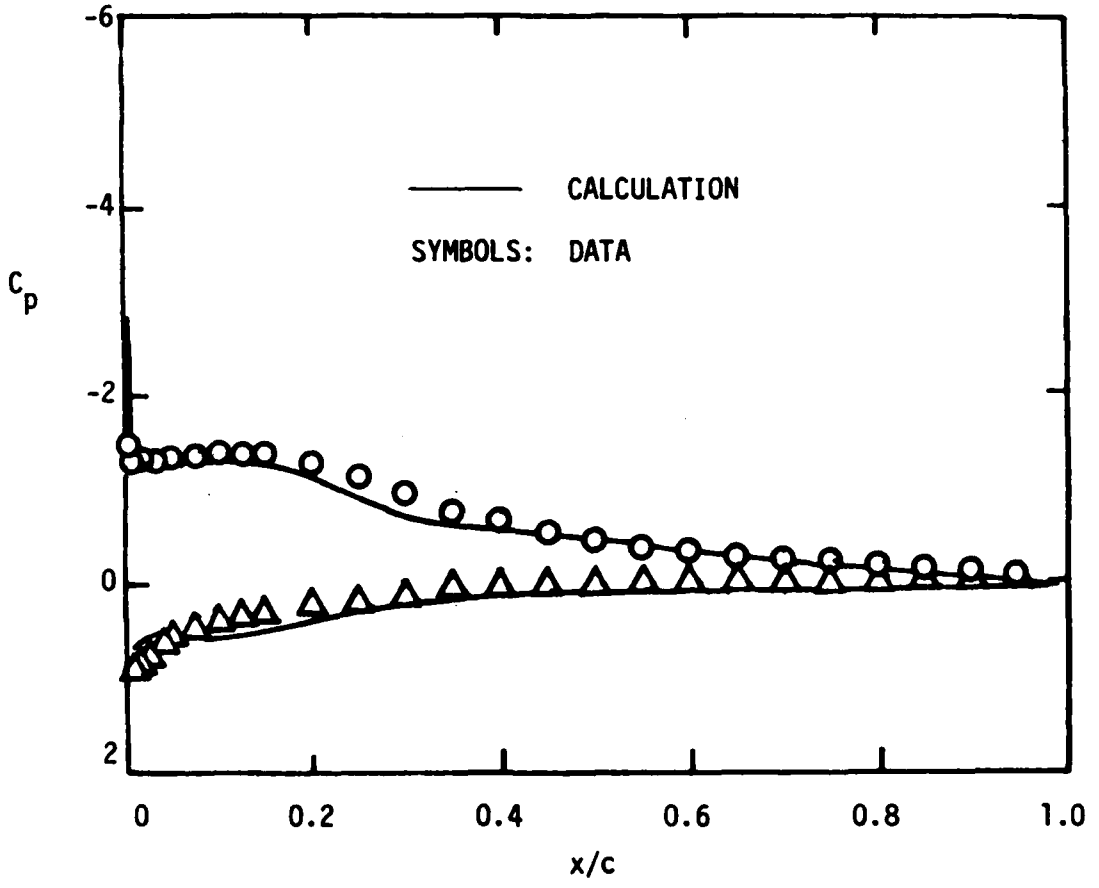

Figure 10. Overall Pressure Distribution on NACA 64A006; $\alpha = 7°$.

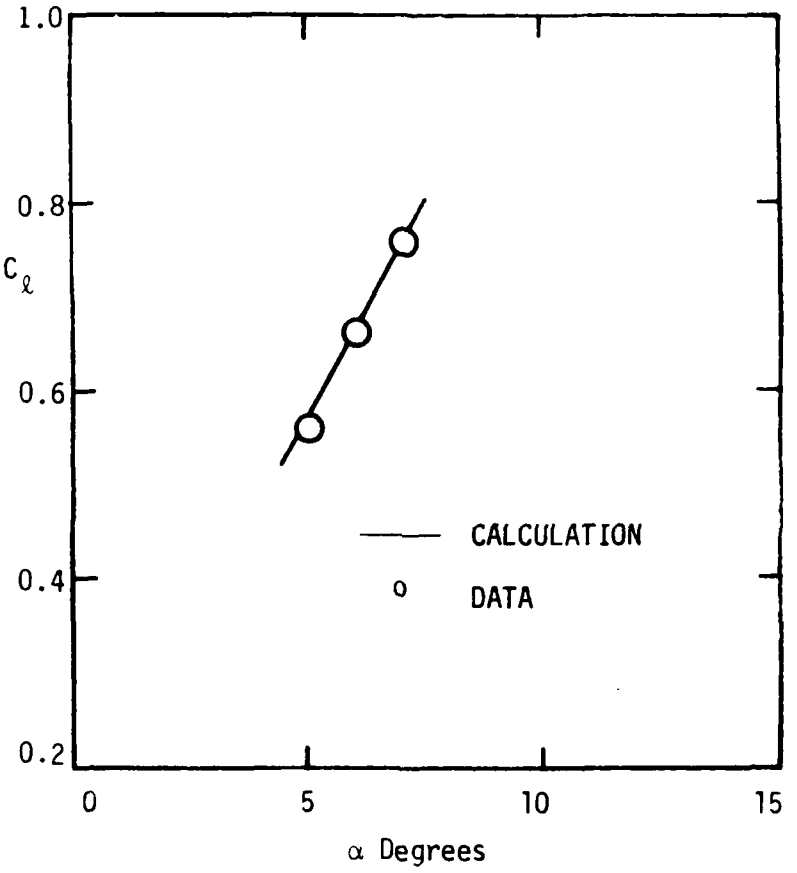

Figure 11. C_ℓ - α Curve for an Airfoil Section NACA 64A006; Re = 5.8 x 10^6.

The overall results presented here are quite good. Even better correlation might have been obtained had the calculation gone one more iteration. One critical area that needs further study is the criterion for identifying the onset of transition to turbulent flow inside the bubble. Relying completely on the displacement thickness at the separation point and the local velocity profile as is done by Crimi/Reeves may make the overall calculation unstable as the resulting velocity profiles in the inverse boundary layer calculation are very sensitive to the boundary layer displacement thickness distribution. Perhaps the boundary layer displacement prescribed along the bubble should be more closely related to the convergence criteria. The effect of the boundary layer displacement thickness distribution on the velocity profile in the separation zone needs to be examined more carefully in a future study.

6.0 RECOMMENDATIONS FOR FUTURE WORK

It has been demonstrated in this work that the leading-edge separation bubble can be analysed by a viscous/potential flow iterative procedure. As described in the previous section the correlation with the data is encouraging. However, there is considerable room for improvement in the calculation procedure to make it more useful and practical.

The future success of the calculation procedure hinges on the accurate prediction of the onset of transition. The transition criterion inside the bubble needs to be improved as the current one, which is based on the relationship between the local velocity profile and the boundary layer displacement thickness at the separation point, predicts early transition. There are two possible reasons for this premature transition. Firstly, the Crimi/Reeves procedure itself may not be valid for the long bubble. Secondly, the velocity profile obtained from the inverse boundary layer calculation in the region of interest may be in appreciable error and thus invalidates the transition test. These uncertainties can be clarified by the following means: a correlation study between the Crimi/Reeves criterion and the existing long bubble data, and a sensitivity test on the boundary layer velocity profiles against the displacement thickness distribution. It may also be desirable to compare the present boundary layer method with other methods, e.g., Horton's inverse boundary layer method (18).

The speed of convergence of the current iterative procedure in obtaining the potential flow calculation is relatively slow. More work is needed in this area to optimize the convergence process.

7.0 REFERENCES

1. McCullough, G.B. and Gault, D.E., "Examples of Three Representative Types of Airfoil-Suction Stall at Low Speed", NACA TN 2502, September 1951.

2. Roberts, W.B., "Calculation of Laminar Separation Bubbles and their Effect on Airfoil Performance", AIAA J., Vol. 18, No. 1, January 1980.

3. Vatsa, V.N. and Carter, J.E., "Analysis of Airfoil Leading-Edge Separation Bubbles", AIAA-83-0300, AIAA 21st Aerospace Sciences Meeting, Reno, Nevada, January 10-13, 1983.

4. Kwon, O.K. and Pletcher, R.H., "Prediction of Subsonic Separation Bubbles on Airfoils by Viscous-Inviscid Interaction", Second Symposium on Numerical and Physical Aspects of Aerodynamic Flow, California State University, Long Beach, California, January 17-20, 1983.

5. Johnson, D.A., Horstman, C.C. and Bachalo, W.D., "Comparison between Experiment and Prediction for a Transonic Separated Flow", AIAA J., Vol. 20, No. 6, June 1982.

6. Cebeci, T., "The Calculation of Momentum and Heat Transfer in Internal Flows and in Flows with Small Regions of Separation", ONR-CR-297-002-1, December 1978.

7. Maskew, B., "Prediction of Subsonic Aerodynamic Characteristics: A Case for Low-Order Panel Methods", J. Aircraft, Vol. 19, No. 2, February 1982.

8. Keller, H.B., A New Finite-Difference Scheme for Parabolic Problems in Numerical Solution of Partial Differential Equations, Ed., J. Bramble, Vol. 2, Academic Press, 1970.

9. Cebeci, T. and Smith, A.M.O., Analysis of Turbulent Boundary Layers, Academic Press, 1974.

10. Granville, P.S., "The Calculation of the Viscous Drag of Bodies of Revolution", David W. Taylor Model Basin Report 849, 1953.

11. Crimi, P. and Reeves, B.L., "Analysis of Leading-Edge Separation Bubbles on Airfoils", AIAA J., Vol. 14, No. 11, November 1976.

12. Smith, A.M.O., "Transition, Pressure Gradient and Stability Theory", Proc. 9th International Congress of Applied Mechanics, Brussels, Vol. 7, 1957.

13. Keller, H.B., "Accurate Difference Methods for Nonlinear Two-Point Boundary Value Problems", SIAM J. Num. Anal., 11:305-20, 1974.

14. Reyhner, T.A. and Flügge-Lotz, I., "The Interaction of a Shock Wave with a Laminar Boundary Layer", Int. J. Non-Linear Mech., 3:173-199, 1968.

15. Howarth, L., "On the Calculation of the Steady Flow in the Boundary near the Surface of a Cylinder in a Stream", ARC R&M 1632, 1935.

16. Gaster, M., "The Structure and Behavior of Laminar Separation Bubbles", NPL Aero Report 1181, March 1967.

17. Gault, D.E., "An Experimental Investigation of Regions of Separated Laminar Flow", NACA TN 3505, September 1955.

18. Horton, H.P., "Comparison between Inverse Boundary Layer Calculations and Detailed Measurements in Laminar Separated Flows", Aero. Quart., Vol. XXXII, August 1981.

END

FILMED

6-85

DTIC